

Letter of intent; Precise measurements of very forward particle production at RHIC

Y.Itow, H.Menjo, G.Mitsuka, T.Sako

Solar-Terrestrial Environment Laboratory / Kobayashi-Maskawa Institute for the Origin
of Particles and the Universe / Graduate School of Science, Nagoya University, Japan

K.Kasahara, T.Suzuki, S.Torii

Waseda University, Japan

O.Adriani, A.Tricomi

INFN, Italy

Y.Goto

Riken BNL, Japan

K.Tanida

Seoul National University

ABSTRACT

In this letter of intent, we propose an experiment for the precise measurements of very forward particle production at RHIC. The proposal is to install a LHCf-like calorimeter in the ZDC installation slot at one of the RHIC interaction points. By installing a high-resolution electromagnetic calorimeter at this location we measure the spectra of photons, neutrons and π^0 at pseudorapidity $\eta > 6$.

The new measurements at 500 GeV p-p collisions contribute to improve the hadronic interaction models used in the cosmic-ray air shower simulations. Using a similar kinematic coverage at RHIC to that of the measurements at LHC 7–14 TeV p-p collisions, we can test the Feynman scaling with a wide \sqrt{s} range and make the extrapolation of models into cosmic-ray energy more reliable. Combination of a high position resolution of the LHCf detector and a high energy resolution of the ZDC makes it possible to determine p_T of forward neutrons with the ever best resolution. This enables us to study the forward neutron spin asymmetry discovered at RHIC in more detail.

Another new experiment expected at RHIC is world-first light-ion collisions. Cosmic-ray interaction models have been so far tested with accelerator data, but colliders have provided only p-p (or \bar{p}) and heavy-ion collisions. To simulate the interaction between cosmic-ray particles and atmosphere, collision of light ions like nitrogen is a ultimate goal for the cosmic-ray physics. We propose 200 GeV p-N collisions together with 200 GeV p-p collisions to study the nuclear effects in the forward particle production.

The experiment can be performed by using the existing LHCf detector. Considering the geometry and response of one of the LHCf detectors, we propose some short dedicated operations. For the particle spectrum and nuclear effect measurements, we need several hours of operation at each condition with ideal luminosities $6 \times 10^{29} \text{ cm}^{-2} \text{ s}^{-1}$, $4 \times 10^{31} \text{ cm}^{-2} \text{ s}^{-1}$ and $7 \times 10^{30} \text{ cm}^{-2} \text{ s}^{-1}$ at 500 GeV p-p, 200 GeV p-p and 200 GeV p-N collisions, respectively. We require collisions of unsqueezed beams to reduce the angular divergence at collisions. For the spin asymmetry measurement, we require 11 hours of operation at 500 GeV p-p collisions with a luminosity $2.5 \times 10^{30} \text{ cm}^{-2} \text{ s}^{-1}$. Horizontal spin polarization is also required.

Our basic idea is to bring one of the LHCf detectors to RHIC after the LHC 13 TeV p-p collision runs planned in early 2015, and then operate from 2016 season at RHIC.

Contents

1	Introduction	4
2	Physics	10
2.1	\sqrt{s} scaling of hadronic interaction	10
2.2	Nuclear effect in atmospheric nuclei	11
2.3	Spin asymmetry measurement	15
3	Experimental setup and detector	19
3.1	Experimental site and location	19
3.2	Detector and data taking	19
4	Sensitivity	22
4.1	Basic performance	22
4.2	Sensitivity in 500 GeV p-p collisions	23
4.3	Sensitivity in 200 GeV p-N collisions	27
5	Beam condition and requirements	29
5.1	Beam condition and operation time	29
5.2	Other requirements	30
6	Schedule and budget	32
A	Addendum	35

Chapter 1

Introduction

Improving cosmic-ray air shower simulation

The origin of cosmic rays is a century-standing problem. Recent observations of ultra-high-energy cosmic rays (UHECR) by the Pierre Auger Observatory (PAO) [1] and Telescope Array [2] have been dramatically improved in both the statistics and the systematics. The existence of a spectral cutoff at approximately $10^{19.5}$ eV is now clearly identified. However, the interpretation of the observed results is not settled. One of the main reasons for the difficulty is the uncertainty in air shower modeling. Fig.1.1 shows the so-called X_{max} parameter as a function of the cosmic-ray energy observed by the PAO. Here, X_{max} is the height of the shower maximum measured from the top of the atmosphere in g/cm^2 . Experimental data are compared with the predictions by air shower simulation with the two extreme assumptions that all cosmic rays are protons or iron nuclei. Four lines in each assumption are due to the use of different interaction models in the air shower simulation. Because of the fact that the difference between models is larger than the experimental errors, the determination of the primary chemical composition is difficult, and hence, the nature of the spectral cutoff is not concluded. The determination of the chemical composition at 10^{17} eV is also important because, at approximately this energy, the source of the cosmic rays is believed to switch from galactic to extragalactic and the chemical composition rapidly changes with energy [3]. However, due to the uncertainty in air shower modeling, the determination of the chemical composition at this energy range is still model dependent. To solve the origin of mysterious UHECRs and to confirm the standard scenario of the cosmic-ray origin, constraints from the accelerator experiments are indispensable.

The difficulty in modeling hadronic interactions, which is essential to determine the air shower development, is due to the difficulty in modeling the soft interaction described by non-perturbative QCD. Experimentally, particles produced in such processes have a large energy flux in the forward direction and are difficult to measure es-

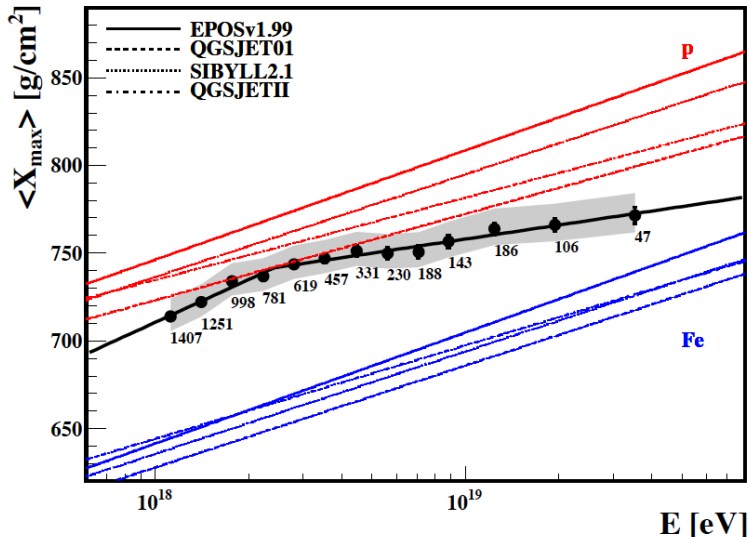


Figure 1.1: X_{max} of air showers observed by the Pierre Auger Observatory. [1]

pecially in the collider experiments. Cosmic-ray interaction models have been tested with a variety of accelerator experiments with a limited number of forward measurements, and most of the data thus far are limited in proton-proton (or anti-proton) collisions. The Large Hadron Collider (LHC) provides an unprecedented quality of test data; this facility gives the highest collision energy, and the experiments cover a very wide range of pseudorapidity (η) [4]. The same quality of lower-energy collision data is very important to test the \sqrt{s} dependence of hadronic interactions to extrapolate the models into the UHECR energy region. In contrast to p-p collisions, only d-Au collisions at RHIC and p-Pb collisions at LHC provide collision situations that are similar to cosmic-ray protons interacting with the atmosphere. In both cases, strong nuclear effects were reported by STAR [5] and ALICE [6]. These effects will be important inputs to simulate proton-atmosphere collisions at extreme conditions. However, no direct tests of nuclear effects in proton-atmosphere collisions have been performed thus far.

Large Hadron Collider forward (LHCf) is one of the LHC experiments to measure forward neutral particles to calibrate the interaction models used in the cosmic-ray physics [7]. LHCf successfully acquired to take data for LHC 900 GeV, 2.76 TeV and 7 TeV proton-proton collisions and 5.0 TeV ($\sqrt{s_{NN}}$) p-Pb collisions. LHCf installed compact calorimeters at the installation slot of the Zero Degree Calorimeter (ZDC) located 140 m from an interaction point of the LHC. Two independent detectors

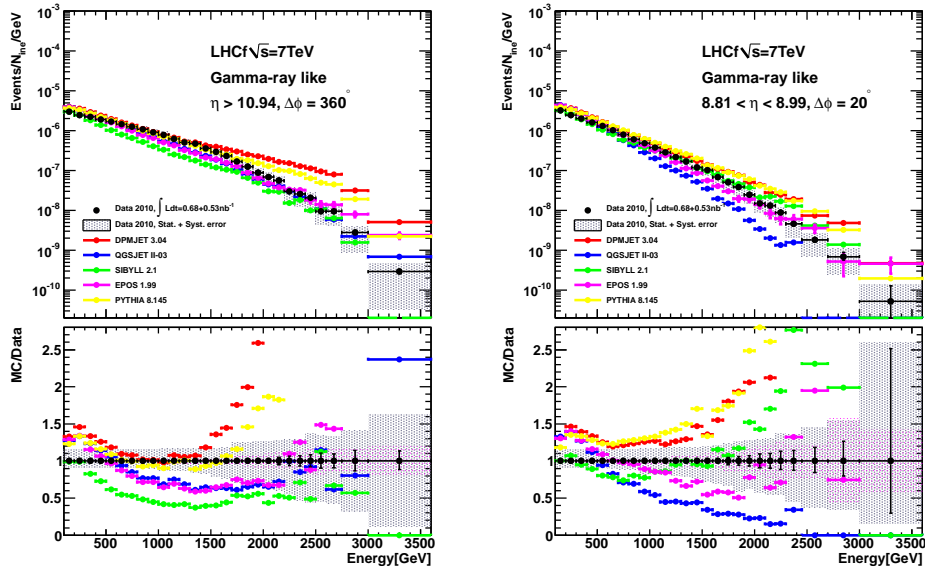


Figure 1.2: Forward photon spectra measured by LHCf at the LHC 7 TeV p-p collisions.

called Arm1 and Arm2 at either side of the interaction point were installed. At this location, neutral particles (predominantly photons decayed from π^0 and neutrons) emitted at $\eta > 8.4$ are observed. Each detector has two small calorimeter towers that allow simultaneous detection of two high-energy particles and hence identification of photon pairs originating from π^0 by reconstructing the invariant mass of these particles. The calorimeters are optimized to measure TeV photons and have energy and position resolutions of $8\%/\sqrt{E/100\text{ GeV}} + 1\%$ and $< 200\ \mu\text{m}$, respectively, in the LHC environment. These dedicated electromagnetic calorimeters enabled the first high-resolution measurements of electromagnetic showers at approximately zero degrees at colliders. These measurements are motivated by the desire to constrain the source of the mesonic branch in an air shower, but it is also possible to access the baryonic part by measuring forward neutrons with limited resolutions. Thus far, LHCf has published energy spectra of forward photons at 900 GeV [8] and 7 TeV [9] and forward π^0 spectra at 7 TeV [10] as shown in Fig.1.2 and Fig.1.3. Generally, no interaction model perfectly explains the LHCf results, but the models bracket the experimental data well. As mentioned above, comparisons of data at different collision energies are essentially important, but a small p_T coverage in the 900 GeV collision data does not allow an effective comparison with the 7 TeV data.

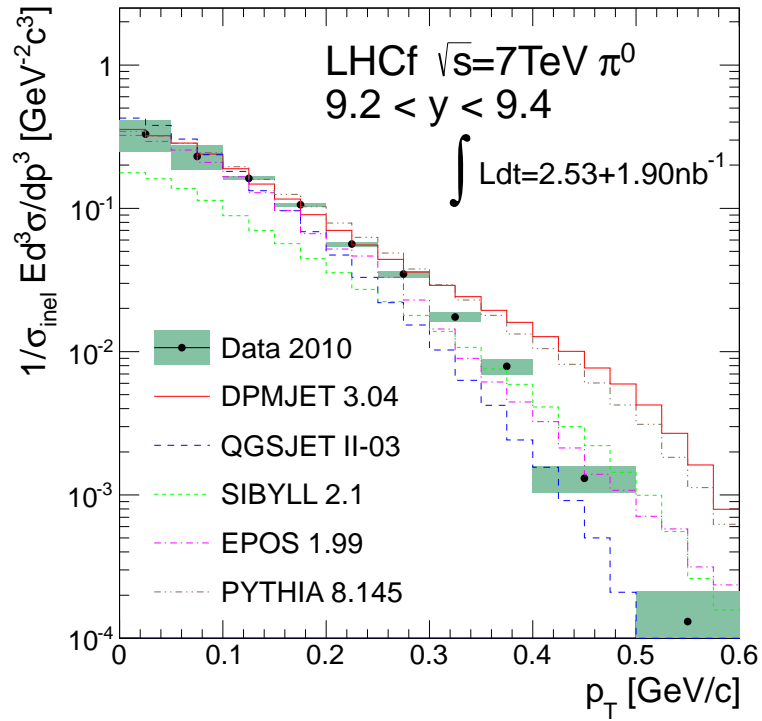


Figure 1.3: An example of forward π^0 spectra measured by LHCf at the LHC 7 TeV p-p collisions.

Extended measurements of forward neutron spin asymmetry

With the first polarized p-p collisions at $\sqrt{s} = 200$ GeV at RHIC, a large single transverse-spin asymmetry (A_N) for neutron production in very forward kinematics was discovered by a polarimeter development experiment [11]. The discovery of the large A_N for neutron production is new, important information to understand the production mechanism of the very forward neutron.

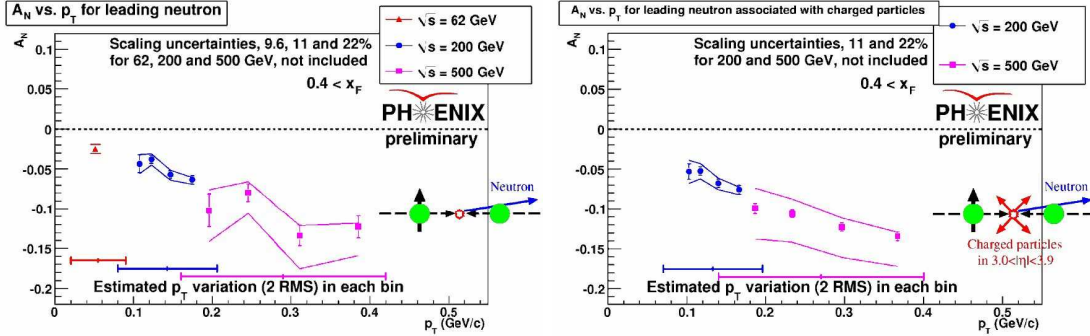


Figure 1.4: The measured asymmetries of very forward neutron production as functions of p_T with an inclusive-neutron trigger (left) and with a semi-inclusive neutron trigger including a beam-beam interaction requirement (right).

The \sqrt{s} dependence of A_N from three different collision energies, 62.4 GeV, 200 GeV, and 500 GeV was studied. The result is shown in Fig. 1.4. The hit position dependence on the detector was measured at each energy, although this dependence was largely smeared by the position resolution. The result was converted to the p_T dependence, which showed a hint of the p_T scaling property of A_N of the very forward neutron production. The asymmetry is caused by interference between spin-flip and non-flip amplitudes with a relative phase. Kopeliovich et al. [12] studied the interference of a pion and a_1 , or a pion and ρ in the 1^+S state. The data agreed well with the independence of energy. The asymmetry is sensitive to the presence of different mechanisms, e.g., Reggeon exchange with spin-non-flip amplitudes even if these amplitudes are small.

In this letter of intent, we propose an experiment like LHCf to be performed at the Relativistic Heavy Ion Collider at BNL to improve modeling of air shower simulations and understanding of the nature of the forward neutron spin asymmetry. By installing a high-resolution electromagnetic calorimeter at the ZDC installation

slot of RHIC, particle production at approximately zero degrees is studied with unprecedented resolutions. The proposed experiment is temporally called RHICf in this letter.

Chapter 2

Physics

At RHIC, the ZDC installation slot is located at 18 m from the IP. The 10 cm gap between beam pipes allows the installation of a LHCf detector itself and measurements of forward neutral particles down to $\eta=6$. Here, we discuss physics of neutral particle measurements at $\eta > 6$ at the RHIC energy. Three advantages, two related to cosmic-ray physics and one for spin asymmetry, are introduced. The details of the detector configuration are discussed in Chap.3.

2.1 \sqrt{s} scaling of hadronic interaction

Fig.2.1 shows the energy spectra of all π^0 at $\sqrt{s}= 500$ GeV, 7 TeV and 50 TeV ($E_{lab} = 1.3 \times 10^{18}$ eV) predicted by the DPMJET3 and QGSJET-II [14] models. With the particle energy scaled by the beam energy (\sim Feynman X, x_F), the DPMJET3 model assumes a perfect Feynman scaling [15], whereas QGSJET-II shows a softening in higher energy collisions. The assumption of the Feynman scaling or collision energy dependence is an important issue to be tested at the collider experiments. Fig.2.2 shows the photon spectra, $d^2N/dp_T/dE$, in the energy- p_T plane predicted by the DPMJET3 interaction model [13] for $\sqrt{s}= 500$ GeV, 900 GeV and 7 TeV proton-proton collisions. The red triangles indicate the phase spaces $\eta > 6.0$ for 500 GeV and $\eta > 8.4$ for the other energies corresponding to the RHICf and LHCf cases, respectively. The phase-space coverage is very similar between 500 GeV at RHIC and 7 TeV at LHC, but is very narrow in the LHC 900 GeV case. The wide and similar coverage of RHIC 500 GeV p-p collisions and LHC 7-14 TeV p-p collisions provides a strong constraint for the Feynman scaling hypothesis that is important to extrapolate the interaction models into the UHECR region.

The configuration at RHIC allows the identification of π^0 using the double towers of the LHCf detector. The minimum opening angle of a photon pair decayed from a

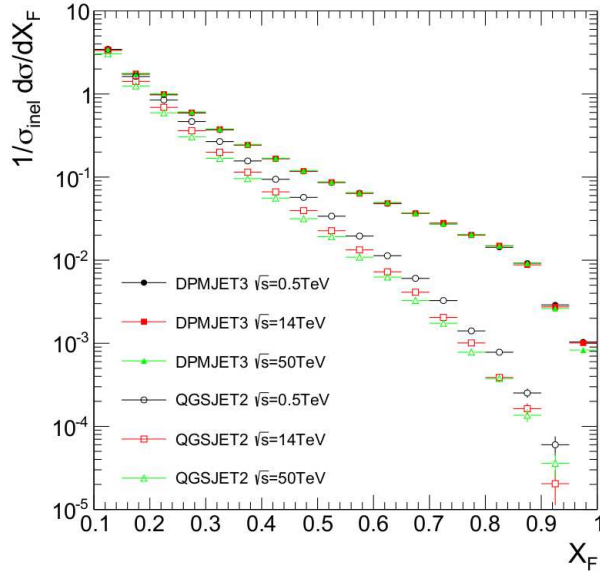


Figure 2.1: X_F spectra of all π^0 at $\sqrt{s} = 500$ GeV, 7 TeV and 50 TeV p-p collisions.

π^0 of energy E is described as $\theta_{min} = 2M/E$, where M is the rest mass of π^0 . In case of 900 GeV p-p collisions at LHC, $\theta_{min} = 600 \mu\text{rad}$ is close to the maximum aperture of the LHCf detector (90 mm/140 m) and no photon pair is identified. However, in the 500 GeV p-p collision at RHIC, $\theta_{min} \sim 1 \text{ mrad}$ is sufficiently smaller than the RHICf aperture (90 mm/18 m = 5 mrad) to allow the detection of photon pairs. Very forward π^0 production was measured by the UA7 experiment for Sp \bar{p} S 630 GeV proton-antiproton collisions [16]. Because UA7 covered slightly higher p_T than the RHICf configuration at similar collision energy, RHICf can provide complementary information to understand the meson production spectrum.

2.2 Nuclear effect in atmospheric nuclei

Direct collider measurements of light ions are expected for cosmic-ray physics, and RHIC is expected to realize the first light-ion collision. Because the nuclear effect is not explicitly implemented in the models, some steps are necessary to clarify the model dependence of the nuclear effect. Fig.2.3 shows energy spectra of π^0 and neutrons at $\eta > 6$ of $\sqrt{s_{NN}} = 200$ GeV p-N collisions using three interaction models, DPMJET3, QGSJET II and EPOS [17]. Here ‘N’ designates nitrogen. As references, spectra in the p-p collisions using the same models in the same rapidity range are

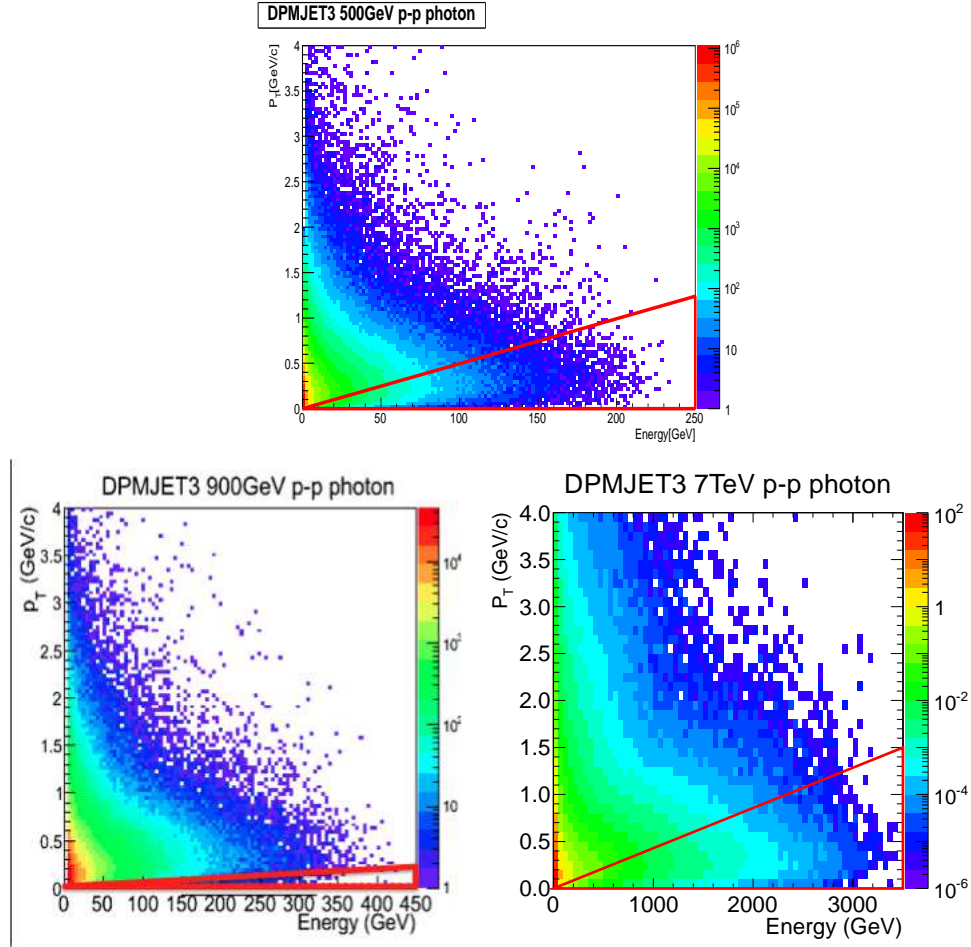


Figure 2.2: Photon yield in the energy- p_T phase space at $\sqrt{s}=500$ GeV, 900 GeV and 7 TeV p-p collisions predicted by the DPMJET3 model. Red triangles indicate the geometrical acceptances of a LHCf-like experiment installed at RHIC in 500 GeV and at LHC in 900 GeV and 7 TeV collisions.

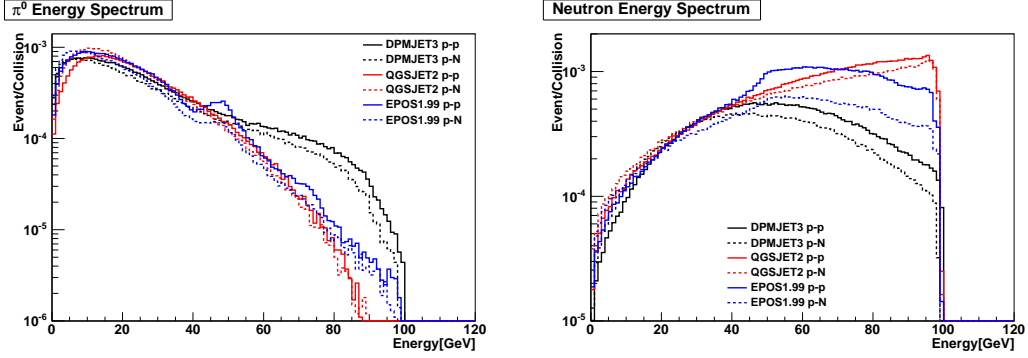


Figure 2.3: Energy spectra of photons (left) and neutrons (right) found at $\eta > 6$ of the proton remnant side in $\sqrt{s_{NN}}=200$ GeV p-nitrogen collisions predicted by the DPMJET3, QGSJET-II and EPOS models. As references, the same spectra in the p-p collisions are also indicated by dashed lines.

also shown. The ratio, R_{model} , of the spectra in p-N collisions to those in p-p collisions are shown in Fig.2.4. These ratios are thought to represent the nuclear effect implemented in each model. To enhance the difference between models, double-ratio spectra $R_{QGSJETII}/R_{DPMJET3}$ and $R_{EPOS}/R_{DPMJET3}$ are shown in Fig.2.5. The results indicate that QGSJET II and EPOS assume similar nuclear effects in the π^0 production spectrum but are different in amplitude at approximately a 20% level. However, QGSJET II and EPOS predict harder and softer neutron spectra, respectively, than DPMJET3, with a 40% difference. The nuclear effect of the very forward particle production in light-ion collisions is a very new field and is never tested in the collider experiments. Experimental verification of different model predictions becomes possible for the first time at RHIC.

Information from the central detectors and the ZDC indicating the impact parameter (b) of the collision will help to explore the fundamental process. As shown in Fig.2.6, the particle spectra produced in peripheral collisions – here, $b > 2.5$ fm – are approximately identical to those of p-p collisions. However, the particles produced in the collisions of $b < 2.5$ fm suffer from multiple collisions in the nuclei. Some indicators of the impact parameter are useful to enhance the effect of multiple collisions.

To complete the possible cosmic-ray and atmosphere interactions, N-N and Fe-N collisions are also interesting as future options. Studying the nuclear effects of light-ion collisions can generally contribute to the physics of cold nuclear matter. The inclusion of p-Pb collision data at the LHC and possible p-Au collisions at RHIC will provide very wide coverage of the nuclear effect in both the mass (A) and energy

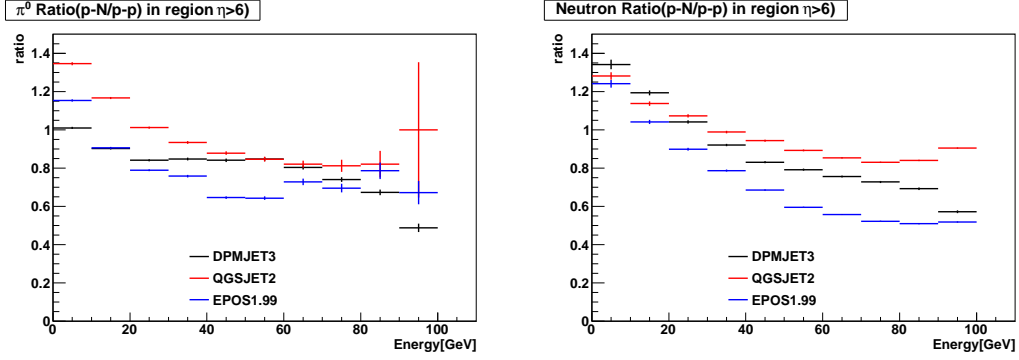


Figure 2.4: Nuclear effect by different models. The left figure is for photons, and the right figure is for neutrons. Definition in the text.

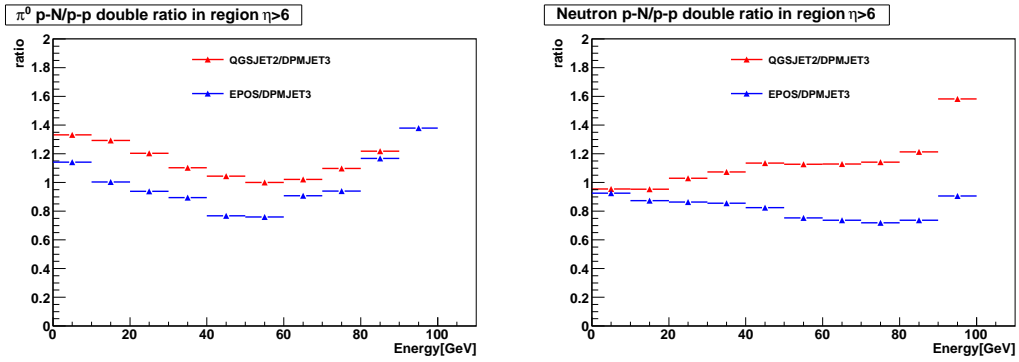


Figure 2.5: Double ratios of the nuclear effect. The left figure is for photons and the right figure is for neutrons.

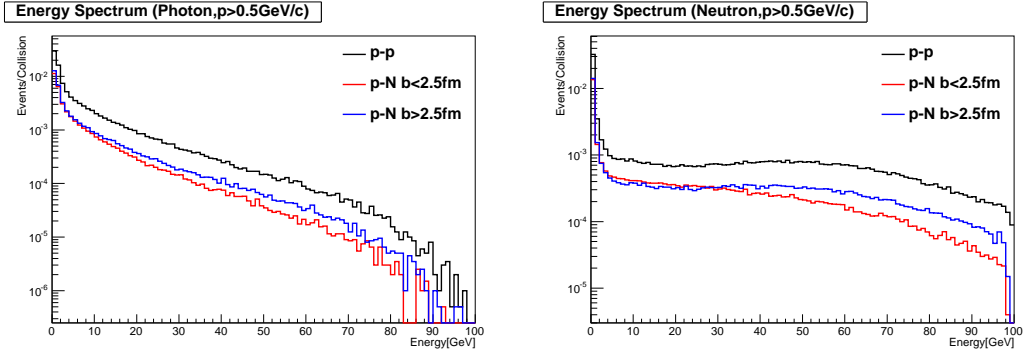


Figure 2.6: Forward particle spectra for the interaction of $b < 2.5$ fm and $b > 2.5$ fm where b indicates the impact parameter.

(E) spaces.

2.3 Spin asymmetry measurement

The origin of the nucleon spin $1/2$ has been investigated with polarized p-p collisions at RHIC. With the first polarized p-p collisions at $\sqrt{s} = 200$ GeV at RHIC, a large single transverse-spin asymmetry (A_N) for neutron production in very forward kinematics was discovered by a polarimeter development experiment [11]. The discovery of the large A_N for neutron production is new, important information to understand the production mechanism of the very forward neutron. The cross section of very forward neutron production was measured at ISR and Fermilab [18]. These researchers measured a forward peak in the x_F distribution around $x_F = 0.8$ and found only a small \sqrt{s} dependence. The cross section was also measured at HERA in e-p collisions [19]. These researchers found a suppression of the forward peak. CERN-NA49 measured the very forward neutron cross section in the p-p reaction [20]. These researchers' cross section was twice large as those measured at ISR and Fermilab, and was consistent with that at HERA. To understand the production mechanism of the forward neutron, more data are necessary, and the asymmetry measurement gives new information.

The cross section and A_N of very forward neutron production in polarized p-p collisions was measured at PHENIX with a ZDC by adding a position-sensitive SMD (Shower Maximum Detector) [21]. The detectors are located downstream of the RHIC-DX dipole magnet so that charged particles from collisions are swept out. As a beam luminosity monitor, beam beam counters (BBCs) are used. These counters

are mounted around the beam pipe located ± 144 cm away from the collision point and cover $\pm(3.0-3.9)$ and 2π in the pseudorapidity and azimuth spaces, respectively. The data was collected by two sets of triggers for the neutron measurement. One trigger was the ZDC trigger for neutron-inclusive measurements by requiring energy deposition in either side of the ZDC (the north side or the south side) above 5 GeV. The other trigger was the ZDC \otimes BBC trigger, a coincidence trigger of the ZDC trigger with BBC hits, which were defined as one or more charged particles in both sides of BBCs.

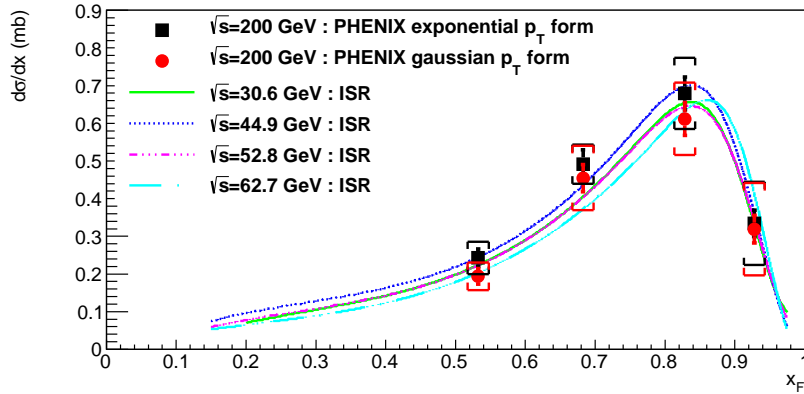


Figure 2.7: The cross section results for forward neutron production in $p + p$ collisions at $\sqrt{s}=200$ GeV are shown. Statistical uncertainties are shown as error bars for each point, and systematic uncertainties are shown as brackets. Absolute normalization errors for the PHENIX and ISR are 9.7% and 20%, respectively.

The differential cross section, $d\sigma/dx_F$, in the integrated p_T region, $0 < p_T < 0.11 \times x_F$ GeV/ c , for forward neutron production in p-p collisions at $\sqrt{s} = 200$ GeV was determined using two p_T distributions: a Gaussian form, as used in the HERA analysis [19], and an exponential form, used for the ISR analysis [18]. The results are plotted in Fig. 2.7. The measured cross section was consistent with the ISR result at \sqrt{s} from 30.6 to 62.7 GeV, indicating that x_F scaling is satisfied at the higher center-of-mass energy.

The single transverse-spin asymmetry with the ZDC trigger was $A_N = -0.061 \pm 0.010(stat) \pm 0.004(syst)$, and that with the ZDC \otimes BBC trigger was $A_N = -0.075 \pm 0.004(stat) \pm 0.004(syst)$. The x_F dependence of the A_N of very forward neutron production is shown in Fig. 2.8. A significant negative A_N was seen in the positive x_F region and there was no energy dependence within the errors in both trigger sets. No significant backward neutron asymmetry was observed.

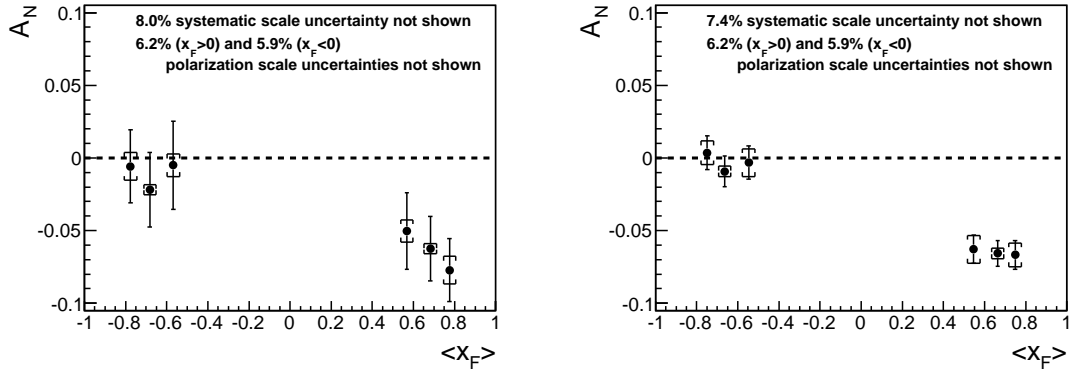


Figure 2.8: The x_F dependence of the A_N for neutron production with the ZDC trigger (left) and with the ZDC \otimes BBC trigger (right). The error bars show statistical uncertainties and brackets show p_T -correlated systematic uncertainties.

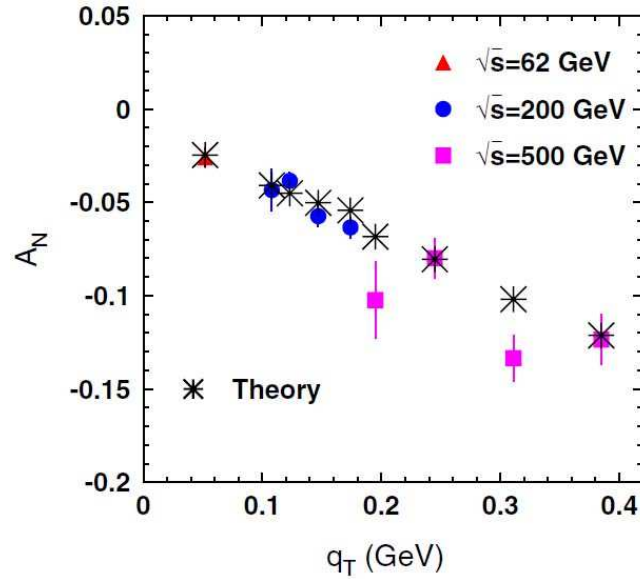


Figure 2.9: The asterisks show the calculation of A_N by Kopeliovich et al. [12] compared with measured A_N at $\sqrt{s} = 62.4$ GeV, 200 GeV, and 500 GeV by the PHENIX experiment.

The \sqrt{s} dependence of A_N from three different collision energies, 62.4 GeV, 200 GeV, and 500 GeV was also studied. The result is shown in Fig. 1.4. The hit position dependence on the detector was measured at each energy, although this dependence was largely smeared by the position resolution. The result was converted to the p_T dependence, which showed a hint of the p_T scaling property of the A_N of the very forward neutron production. The asymmetry is caused by interference between spin-flip and non-flip amplitudes with a relative phase. Kopeliovich et al. [12] studied the interference of a pion and a_1 , or a pion and ρ in the 1^+S state. The data agreed well with the independence of energy, as shown in Fig. 2.9. The asymmetry is sensitive to the presence of different mechanisms, e.g., Reggeon exchange with spin-non-flip amplitudes even if these amplitudes are small.

Advantages of the use of the LHCf detector for cross-section and asymmetry measurements at RHIC are an improved p_T resolution due to the good position resolution of the LHCf detector and a wider p_T coverage due to the detector geometry. Improved p_T information enables us to measure the p_T dependence of the cross-section and the asymmetry and to determine the invariant cross section, which are useful for the study of the production mechanism of forward neutron production as additional and new inputs.

Chapter 3

Experimental setup and detector

3.1 Experimental site and location

To classify the event category, for example, by impact parameter, the information from the other detectors will be useful. From this point of view, installation at the PHENIX or STAR interaction points is preferable. The detector will be installed at the installation location of the ZDC, 18 m from the IP, as shown in Fig.3.1. The 10 cm gap between the beam pipes allows an installation of the existing LHCf detector, whose dimensions are 92 mm (W) \times 290 mm (L) \times 620 mm (H). The detector will be installed on a mechanical structure, a manipulator, that allows the detector to move vertically. The installation of the detector in front of the ZDC requires an agreement with the host experiment and the accelerator operation team. As discussed in Chap.5, because our operation will be completed within a short period, the interference to the ZDC measurement for luminosity determination can be minimized. Using the manipulator, the detector will be placed out of the operation position when RHICf does not take data. The manipulator also allows the position scan during physics runs to enlarge the p_T coverage.

3.2 Detector and data taking

Here, we suppose to use one of the LHCf detectors, Arm1. Any upgrade for optimization to the RHIC condition depends on the schedule, budget and manpower as discussed in Chap.6. The Arm1 detector is composed of calorimeters of 20 mm \times 20 mm and 40 mm \times 40 mm cross sections as shown in Fig.3.2. Each calorimeter has 44 radiation lengths of tungsten in the beam direction. Sixteen layers of sampling scintillator are inserted every two radiation lengths in the first 11 layers and then every four radiation lengths. Four X-Y pairs of position-sensitive layers composed of scintillating

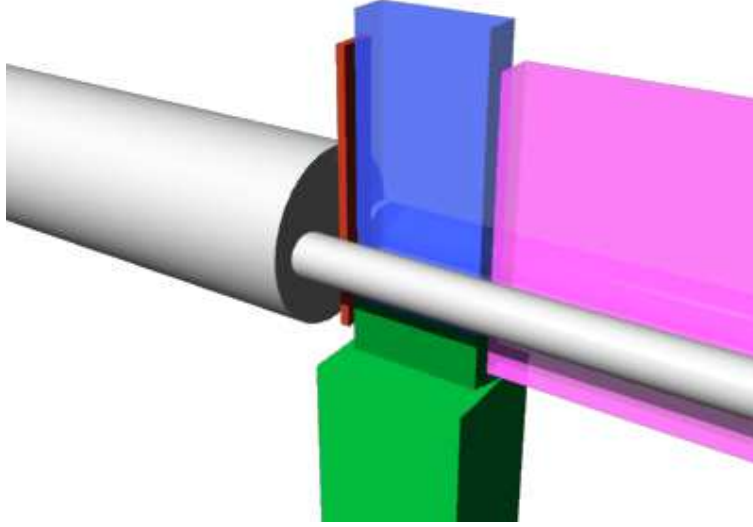


Figure 3.1: Simple drawing to show the installation location and relationship between beam pipes (grey), ZDC (magenta), RHICf (blue) and front detector (red). Green structure indicates the place to install a manipulating lift.

fiber (SciFi, 1 mm \times 1 mm cross section) belts are inserted at the depths of 6, 10, 30 and 42 radiation lengths. Plastic scintillators (EJ-260) and SciFis were used until the 2010 LHC operation but are replaced with Gd₂SiO₅ (GSO) scintillators and GSO bars, respectively, for the LHC 2015 run. This radiation-hard upgrade assures an operation of a LHCf detector at RHIC even after irradiation at LHC in 2015.

Due to the small transverse dimensions, a large fraction of shower particles leak out from the calorimeter. However, because this fraction is known to be a function of only the incident position and is independent from the incident energy, the correct energy can be reconstructed using the information from the position sensitive detector. Because the basic performance is determined by the structure and sampling interval, the difference of scintillator material is not important for performance. The performance of the current plastic scintillator detector for a 50–200 GeV electromagnetic shower was well studied with beam tests at the SPS North area experimental site in CERN [22]. The expected performance at RHIC is discussed in Sec.4.1.

The target of our measurement is neutral particles; however, some contamination from charged particles is expected. To eliminate such contamination, a simple position-sensitive scintillator is planned to be installed in front of the main detector. Any showering event having a hit in the corresponding position of the front detector

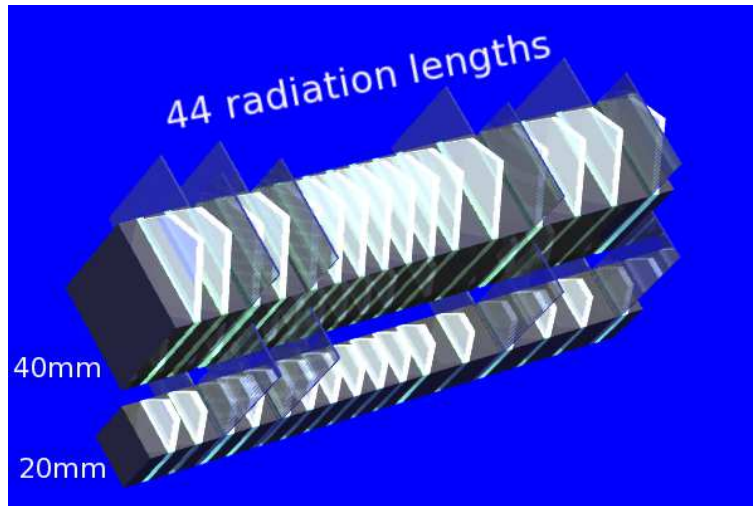


Figure 3.2: Schematic view of the calorimeters in the LHCf Arm1 detector.

is identified as contamination from a charged particle.

Chapter 4

Sensitivity

In this Chapter, the expected spectra considering the detector performance and the acceptance are presented. The performances of the current LHCf detectors were well studied and published in [22]. However, for a more realistic estimation at the RHIC operation, the performance of the upgraded detector using GSO scintillators is introduced here as possible. A new MC study is also important to extract the performance below <100 GeV, which is not in the scope at the LHC operation but important at RHIC. It is important to note that the responses at this energy range can be directly calibrated with the beam test at SPS planned for the end of 2014. A possible improvement in the neutron measurement when combined with the ZDC is also discussed.

4.1 Basic performance

Performances in photon measurements

The energy resolution for the upgraded GSO detector based on the MC simulation is shown in Fig.4.1. The result shows the resolution of 10–3.5% for incident photon energies of 10–200 GeV. The position resolution for the GSO detector is under investigation. The beam test for the SciFi detector showed the position resolution of 150–200 μm for the photon incident of 50–200 GeV [23].

Performances in neutron measurements

The performance for incident neutrons is studied only for the plastic scintillator detector. The energy resolution is 30–35% with very little energy dependence. The incident position is determined with a resolution of 2.4–1.8 mm for incident energies of 100–200 GeV.

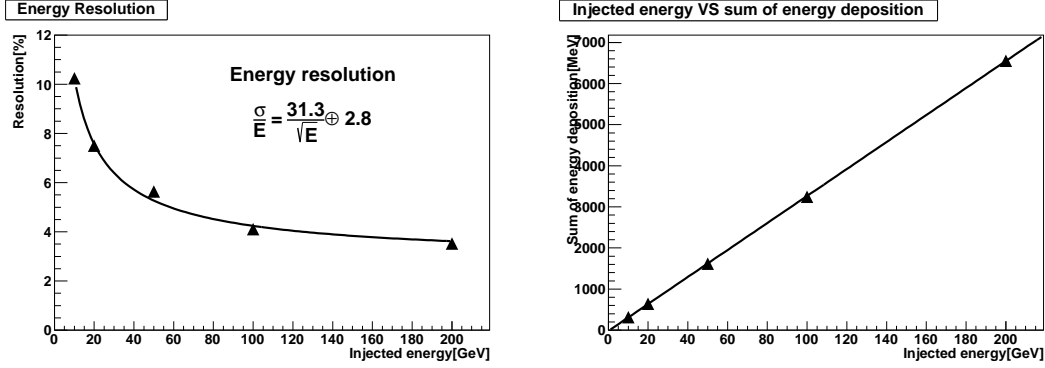


Figure 4.1: Energy resolution (left) and linearity (right) in photon measurements. The results for the GSO detector using MC simulation without electrical noise.

Combination with ZDC

A preliminary study for a combined analysis of RHICf and the ZDC indicates an improvement of the detector performance. When a neutron-induced hadronic shower develops in the RHICf detector, a better position resolution than that of the ZDC as described above is obtained. However, by collecting most of the leaked particles from the small RHICf detector by the ZDC, an energy resolution close to that of the ZDC (20% at 100 GeV) is achieved, as shown in Fig.4.2. Taking advantages of two detectors, a better p_T resolution for neutrons is expected. Fig.4.3 demonstrates the expected p_T resolution as a function of x_F and p_T assuming energy resolution of 20%. Red and blue bars indicate p_T resolutions in cases of the position resolution of 1 mm and 2.5 mm, respectively. The 1 mm resolution is a typical value in the former SMD measurement introduced in Sec.2.3 while 2.5 mm is an expected value in the RHICf experiment. Significant improvement is expected at low to mid p_T range.

4.2 Sensitivity in 500 GeV p-p collisions

According to the DPMJET3 model, in 3.2% of inelastic collisions, a neutral particle of >10 GeV is observed in any of the two calorimeters. In this case, the probability of more than one particle hitting a calorimeter is approximately 1%. Although such multi-hit events are removed from the analysis, and although this removal causes a systematic distortion in the spectral shape, the 1% multi-hit is at an acceptable level.

As discussed in Chap.5, 10^6 particle detections (3×10^7 inelastic collisions at this

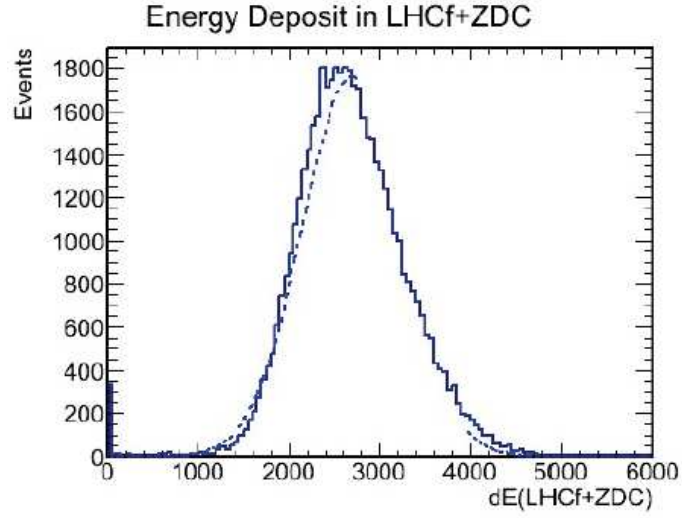


Figure 4.2: Distribution of deposited energy summed over the RHICf and ZDC detectors for 100 GeV neutron incident.

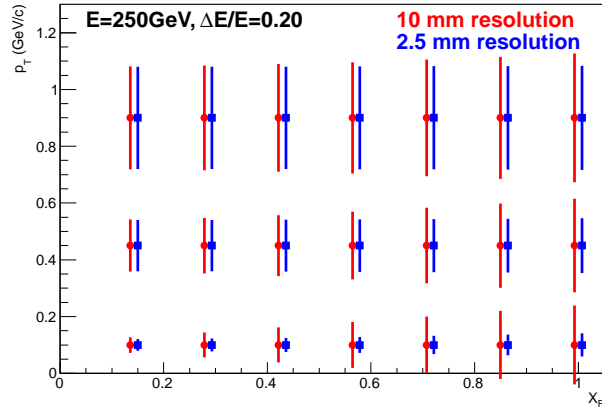


Figure 4.3: p_T resolution as a function of x_F and p_T in cases of position resolution 10 mm (red) and 2.5 mm (blue) corresponding to the former and RHICf measurements, respectively.

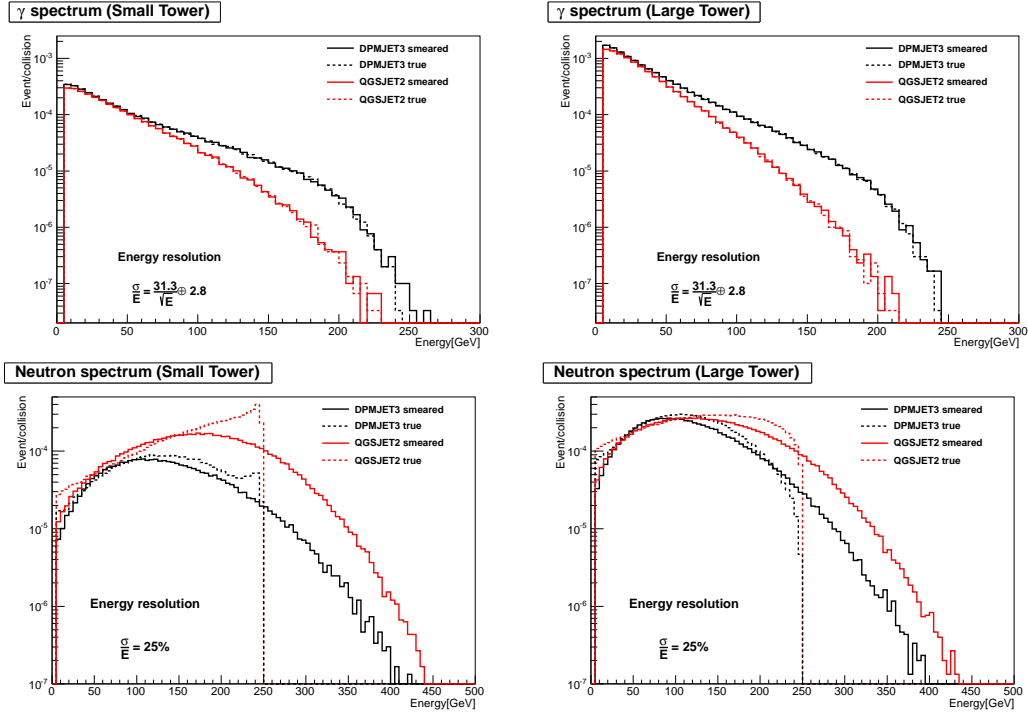


Figure 4.4: Expected photon (top) and neutron (bottom) spectra obtained by the RHICf calorimeters after 3×10^7 inelastic interactions. Left and right histograms show spectra for the small and large calorimeters, respectively. Solid lines are results with energy resolution taken into account while dotted lines without detector response.

collision energy) are assumed as a unit of physics operation. Fig.4.4 shows the expected spectra for photons and neutrons observed in the RHICf calorimeters. The energy resolution discussed in Sec.4.1 is taken into account in the solid histograms. The calculation is performed for the interaction models of DPMJET3 and QGSJET-II. Even considering the detector response, a statistically clear difference is observed. In the same data sample, approximately 1,000 of the π^0 are expected to be identified. The invariant mass spectra of photon pairs are shown in Fig.4.5. By selecting events with invariant mass of 120–150 MeV, the expected π^0 spectra using DPMJET3 and QGSJET-II are extracted as shown in Fig.4.6. There is a statistically clear difference between the two models. To provide a differential cross section in $d^3\sigma/dp^3$, more events are necessary.

The expected numbers of events after 0.1 pb^{-1} of 500 GeV p-p collisions are studied using the PYTHIA minimum-bias event generation. The numbers of inclusive

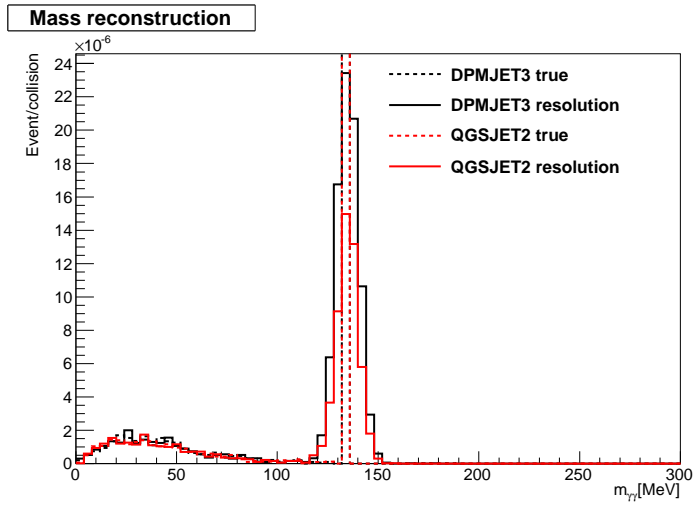


Figure 4.5: Expected invariant mass spectra obtained by the RHICf detector. after 3×10^7 inelastic interactions. Solid and dotted lines for with and without detector response, respectively.

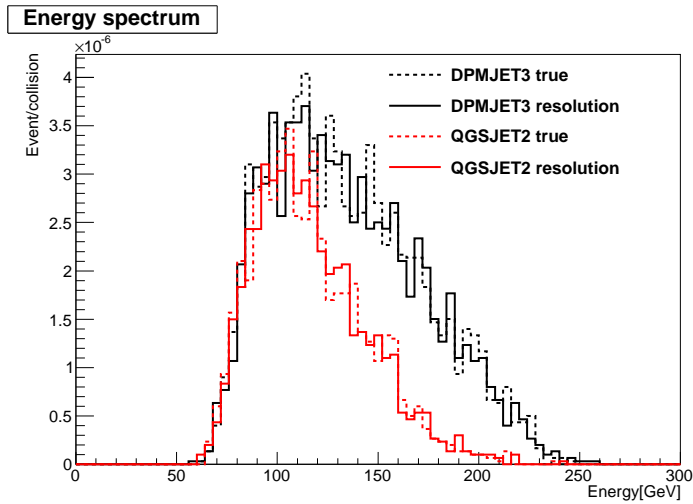


Figure 4.6: Expected π^0 spectra obtained by the RHICf detector after 3×10^7 inelastic interactions. Solid and dotted lines for with and without detector response, respectively.

photons, neutrons, and π^0 at $x_F > 0.4$ accepted in the LHCf detector are summarized in Tab.4.2. The precision of the asymmetry measurement, $\delta A = 1/P \cdot \sqrt{N}$, is also summarize in the table. The polarization P is assumed to be 70%. A 0.1%-level measurement of neutron asymmetry and a 1%-level measurement of π^0 can be performed up to $p_T = 0.7$ GeV/ c .

Table 4.1: Statistics (1,000 events) obtained from 0.1 pb⁻¹ luminosity. δA indicates the expected statistical accuracy of the asymmetry determination.

p_T (GeV/ c)	neutron		photon		π^0	
	N	δA	N	δA	N	δA
0.1 – 0.2	4,790	0.0007	450	0.0021	200	0.0032
0.2 – 0.3	7,030	0.0005	1,220	0.0013	120	0.0041
0.3 – 0.4	10,290	0.0004	1,290	0.0013	160	0.0035
0.4 – 0.5	7,870	0.0005	600	0.0018	150	0.0037
0.5 – 0.6	4,520	0.0007	150	0.0037	70	0.0055
0.6 – 0.7	1,990	0.0010	50	0.0067	20	0.0097

4.3 Sensitivity in 200 GeV p-N collisions

The expected spectra from the 200 GeV p-p and p-N collisions are also studied. The most important difference from the 500 GeV p-p case is the observation at the N-remnant side. In this case, in most of the events, the calorimeters record showers from more than one particle mainly from the fragmentation neutrons. As discussed in Sec.4.2, this high multi-hit rate disables a reliable analysis and the observation at the N-remnant side is not a target of this proposal.

In the p-p and p-N (p-remnant side) collisions, in 0.05% collisions, a single particle is recorded in one of the RHICf calorimeters. The probability of multi-hit contamination is estimated at below 1% and at the acceptable level.

The expected spectra of the p-N/p-p ratio introduced in Sec.2.2 after 2×10^7 collisions are shown in Fig.4.7. Similar trend to Fig.2.4 which does not take into account the experimental effects is clearly visible. It is also noted that Fig.2.4 shows the nuclear effect in the π^0 spectrum but Fig.4.7 is for photons. The difference in the low energy part is due to the background particles produced in the interaction between collision products and beam pipe.

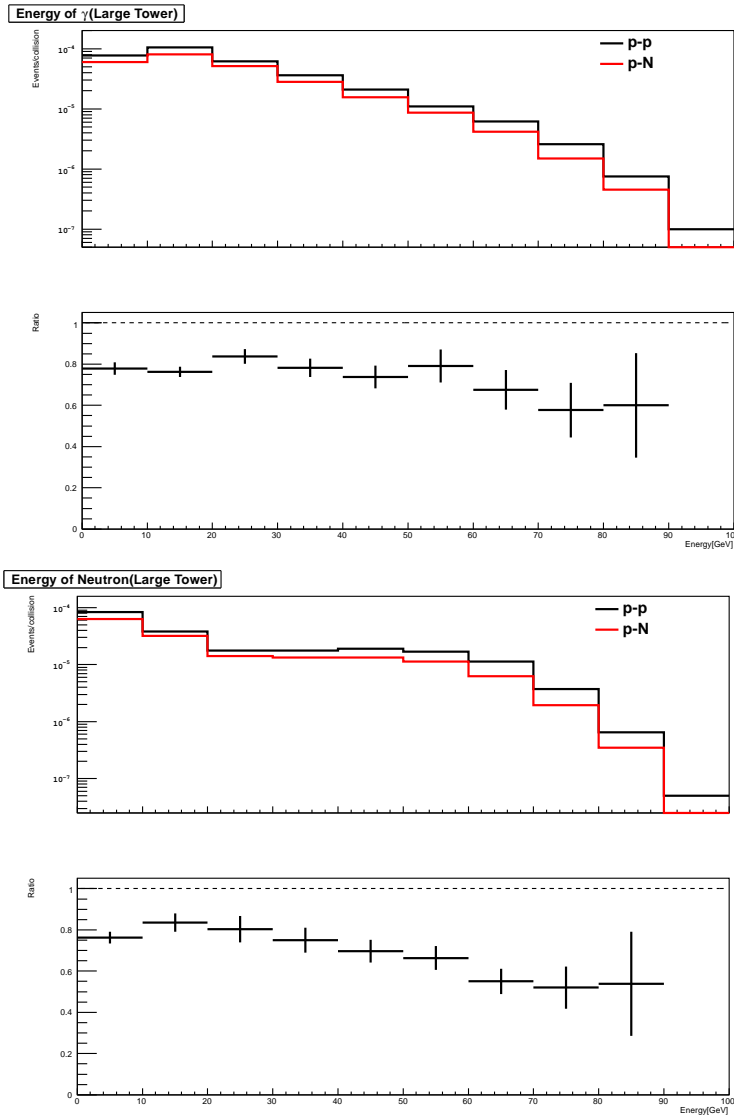


Figure 4.7: Expected spectra of p-N/p-p ratio obtained by the RHICf large calorimeter after 2×10^7 inelastic interactions. Top two plots show the spectra of photons in p-p (black) and p-N (red) collisions and its ratio p-N/p-p. Bottom two plots are for neutrons.

Chapter 5

Beam condition and requirements

5.1 Beam condition and operation time

Assuming the use of the LHCf Arm1 detector for RHICf, the data acquisition speed is limited to 1 kHz. According to the DPMJET3 simulation, the geometrical acceptance of the RHICf detector for >10 GeV neutral particles is 3.2% for an inelastic collision in the case of 500 GeV p-p collisions. This situation requires a desirable collision rate of 31 kHz. Using a cross section of inelastic collision $\sigma_{ine} = 50$ mb, an ideal luminosity is $6.3 \times 10^{29} \text{ cm}^{-2} \text{ s}^{-1}$. To avoid a signal overlap in the shaping amplifier of the MAPMT readout electronics, a desirable interval of events is $> 2 \mu\text{sec}$. This situation requires the maximum number of bunches and the luminosity per bunch to be 6 and $1.1 \times 10^{29} \text{ cm}^{-2} \text{ s}^{-1}$, respectively. The collision pileup $\mu=0.065$, in this case, does not have a significant effect when the detector acceptance of 3.2% is taken into account. It is noted that the $2 \mu\text{sec}$ limit is only to maximize the efficiency. It is possible to identify the overlapped events and remove them at the offline level. A summary of the ideal parameters is given in Tab.5.1 along with the cases of 200 GeV p-p and p-N collisions.

To avoid an angular divergence, higher β^* is needed. A $55 \mu\text{rad}$ divergence of the collision angle results a 1 mm positional divergence on the RHICf detector located 18 m from the IP, which is a sufficient value to use the position resolution of the detector effectively. With the normalized beam emittance ϵ^* , the beam energy E and β^* , the angular beam divergence $\Delta\theta$ at the IP is expressed as

$$\Delta\theta = 136 \mu\text{rad} \times \sqrt{\frac{(\epsilon^*/20 \text{ mm mrad})}{(E/100 \text{ GeV})(\beta^*/10 \text{ m})}}$$

Assuming nominal values $\epsilon^*=20 \text{ mm mrad}$ and $\beta^*=10 \text{ m}$, $\Delta\theta = 136 \mu\text{rad}$ and $86 \mu\text{rad}$ for $E=100 \text{ GeV}$ and 250 GeV , respectively. In the 250 GeV case, the dispersion is

close to the acceptable value, but in the 100 GeV case, a smaller ϵ^* and a larger β^* as possible are preferred.

With the beam condition above (and Tab.5.1), 10^6 events are collected in 1,000 sec that can be a minimum set of physics data to obtain the energy spectra of forward photon and neutrons at each collision energy and beam type. In the actual operation, several sets of 10^6 events (a few hours of operation) are required to perform a position scan and to study the detector systematics. Because of this short operation time and the possible interference with the ZDC as described below, our operation will be performed as special runs.

For the asymmetry measurement, an integrated luminosity of 0.1 pb^{-1} at 500 GeV p-p collisions is required as discussed in Sec.4.2. Assuming a luminosity of $2.5 \times 10^{30} \text{ cm}^{-2} \text{ s}^{-1}$, $4 \times 10^4 \text{ s}$, or approximately 11 hours, are required for data acquisition. To compensate for the slow data acquisition speed at a relatively higher luminosity, we will set a higher trigger threshold to collect only events $>100 \text{ GeV}$. In the neutron asymmetry study, horizontal polarization of the proton beams is required because a wide p_T survey is available only in the vertical direction and up-down asymmetry is expected.

5.2 Other requirements

In all cases, we place the detector in front of the ZDC. Before the collision condition is stabilized, the detector will be placed at the garage position where no interference to the ZDC measurement is expected. Once the stable collision condition is established, the detector is moved in front of the ZDC using the manipulator described in Sec.3. In both the p-p and p-N collision cases, operation of the ZDC is desired. The data behind the RHICf detector will help to improve the energy resolution of neutron events. The data in the N-remnant side, where we do not install a detector, will help to categorize the collisions.

The location to install the readout electronics is an issue for discussion. At the LHC environment, because of the heavy radiation, a large part of the electronics are separated from the detector by 200 m cables. Depending on the radiation condition at RHIC, the installation of approximately 50 cables (each 100 m in length) and space to install readout electronics will be needed. The space and amount of the cables are not large but require additional discussions and arrangements.

To synchronize the readout electronics with the beam, a beam-induced timing signal and a radio frequency clock signal are necessary. Information of the bunch configuration along with the orbit signal are also useful in case the beam timing signal is not available. A flag exchange or a common trigger with the host experiment is also required to allow combined analysis to classify the events and to improve the

Table 5.1: Summary of assumption and requests for beam parameters

	Unit	p-p		p-N (p side)
		500 GeV	200 GeV	200 GeV
RHICf acceptance (ξ)		0.032	5.9×10^{-4}	4.5×10^{-4}
σ_{ine}	mb	50	40	330
emittance (ϵ)	mm mrad	20	<20	<20
β^*	m	10	>10	>10
luminosity (L)	$10^{30} \text{ cm}^{-2} \text{ s}^{-1}$	0.63	42	6.7
number of bunches (n_b)		6	6	6
N_{ine} per bunch crossing (μ)		0.065	3.6	4.7
RHICf event rate ($\xi \sigma_{ine} L$)	Hz	10^3	10^3	10^3
RHICf event pileup ($\mu \xi$)		2.1×10^{-3}	2.1×10^{-3}	2.1×10^{-3}
number of RHICf event (N_{RHICf})		10^6	10^6	10^6
number of collision (N_{ine})	10^8	0.31	17	22
integrated luminosity	nb $^{-1}$	0.63	42	6.7
total time ($N_{ine}/\sigma_{ine}/L$)	sec	10^3	10^3	10^3

energy resolution in the neutron measurement.

Chapter 6

Schedule and budget

Our plan is to bring one of the current LHCf detectors after the LHC 13 TeV p-p collision operation in early 2015 and to be ready for the 2016 RHIC run. Depending on the real schedule of the LHC and the beam species and energy at RHIC, the schedule must be flexible.

The current LHCf detector is available even after the 2015 operation at the LHC thanks to the radiation-hard upgrade using GSO scintillators. A reuse of one of these detectors for the RHIC operation is agreed upon in the LHCf collaboration. The main cost for the detector is solved. However, because the LHCf detectors are optimized for TeV photon detection and use slow readout electronics, several levels of upgrade or the development of another detector optimized for RHIC are discussed as options. Depending on the available budget, a performance improvement from what is described in this letter can be expected.

To allow the vertical movement of the detector, a manipulator is necessary. At the LHC, a manipulator is fixed on the TAN, a neutral particle absorber surrounding the beam pipe around the ZDC slot. Because there is no such structure at RHIC, a dedicated manipulator must be constructed. Because the detector can be held from the bottom in the RHIC situation, a lift type manipulator is possible and can be easily constructed with an approximate cost of 10 kUSD.

Bibliography

- [1] The Pierre Auger Collaboration, PRL, 104, 091101 (2010); The Pierre Auger Collaboration, PLB, 685, 239-246 (2010).
- [2] The Telescope Array Collaboration, Astropart. Phys., 39-40, 109-119 (2012); The Telescope Array Collaboration, International Symposium on Future Directions in UHECR Physics (2012).
- [3] W.D. Apel, *et al.*, Astropart. Phys., **31**, 86-91 (2009).
- [4] D. d'Enterria *et al.*, Astropart. Phys., **35**, 98-113 (2011).
- [5] The STAR Collaboration, Phys. Rev. Lett, **97**, 152302 (2006).
- [6] The ALICE Collaboration, CERN-PH-EP-2012-306 (2012).
- [7] The LHCf Collaboration, Technical Design Report, CERN-LHCC-2006-004 (2006).
- [8] The LHCf Collaboration, Phys. Lett. **B715**, 298-303 (2012).
- [9] The LHCf Collaboration, Phys. Lett. **B703**, 128-134 (2011).
- [10] The LHCf Collaboration, Phys. Rev. **D86**, 092001 (2012).
- [11] Y. Fukao *et al.*, Phys. Lett. **B650**, 325-330 (2007). [hep-ex/0610030].
- [12] B. Z. Kopeliovich, I. K. Potashnikova, I. Schmidt and J. Soffer, Phys. Rev. D **84**, 114012 (2011).
- [13] F.W. Bopp, J. Ranft, R. Engel, S. Roesler, *Phys. Rev. C* **77**, 014904 (2008).
- [14] S. Ostapchenko, *Phys. Rev. D* **74**, 014026 (2006).
- [15] R.P.Feynman, Phys. Rev. Lett., **23**, 24 (1969)
- [16] The UA7 Collaboration, PLB, 242, 531-535 (1990).

- [17] K. Werner, F.-M. Liu, T. Pierog, *Phys. Rev. C* **74**, 044902 (2006).
- [18] J. Engler *et al.*, Nucl. Phys. **B84**, 70 (1975); W. Flauger, F. Monnig, Nucl. Phys. **B109**, 347 (1976).
- [19] S. Chekanov *et al.* [ZEUS Collaboration], Nucl. Phys. **B776**, 1-37 (2007); F. D. Aaron *et al.* [H1 Collaboration], Eur. Phys. J. **C68**, 381-399 (2010).
- [20] T. Anticic *et al.* [NA49 Collaboration], Eur. Phys. J. **C65**, 9-63 (2010). [arXiv:0904.2708 [hep-ex]].
- [21] C. Adler, A. Denisov, E. Garcia, M. J. Murray, H. Strobele, S. N. White, Nucl. Instrum. Meth. **A470**, 488-499 (2001).
- [22] T. Mase *et al.*, Nucl. Instr. Meth., **A671**,129 (2012).
- [23] M.Mizuishi *et al.*, J. Phys. Soc. Jpn. **78** Suppl. A, 173-176 (2009)

Appendix A

Addendum

This appendix is added after the submission of LOI. According to the reference ‘RHIC Collider Projections (FY 2014 – FY 2018), W. Fischer et al.’, we found some of our requested luminosity values were higher than the planned values. We relaxed some of our requirements to be consistent with these values. The average luminosities at 510 GeV p-p collisions, 200 GeV p-p collisions and 200 GeV p-C collisions are documented as

$$1.7 \times 10^{32} \times \left(\frac{\beta^*}{0.65 \text{ m}}\right)^{-1} \left(\frac{n_b}{107}\right) \text{ cm}^{-2} \text{ s}^{-1}$$

$$3.8 \times 10^{31} \times \left(\frac{\beta^*}{0.85 \text{ m}}\right)^{-1} \left(\frac{n_b}{107}\right) \text{ cm}^{-2} \text{ s}^{-1}$$

and

$$7 \times 10^{30} \times \left(\frac{\beta^*}{0.8 \text{ m}}\right)^{-1} \left(\frac{n_b}{111}\right) \text{ cm}^{-2} \text{ s}^{-1}$$

, respectively. The proportional factors to β^* and n_b are added. Though our original proposal is to perform proton-nitrogen collisions, proton-carbon collisions planned in ‘RHIC Collider Projections’ can give us equivalent physics results and then we assume p-C collisions here. Using our requested parameters, $\beta^*=10 \text{ m}$ and $n_b=6$, possible luminosities are $6.2 \times 10^{29} \text{ cm}^{-2} \text{ s}^{-1}$, $1.8 \times 10^{29} \text{ cm}^{-2} \text{ s}^{-1}$ and $3 \times 10^{28} \text{ cm}^{-2} \text{ s}^{-1}$ for 500 GeV p-p collisions, 200 GeV p-p collisions and 200 GeV p-C collisions, respectively. The values for 200 GeV collisions clearly conflict with our ideal luminosities in Tab.5.1.

To be consistent with the values in ‘RHIC Collider Projections,’ we relaxed the $n_b=6$ restriction and consider its effects. Assuming $n_b=100$ and $\beta^*=10 \text{ m}$, $L=3.0 \times 10^{30} \text{ cm}^{-2} \text{ s}^{-1}$ is achieved at 200 GeV p-p collisions. Using the inelastic cross section and RHICf acceptance in Tab.5.1, 71 Hz of event rate is expected. To collect 10^6 events, 3.9 hours of operation is required. Note that Fig.4.7 is produced with 2×10^7 inelastic collisions

corresponding to 10^4 events. Consequently, several hours of operation still provide statistically sufficient number of events.

With the new condition above, the average number of interaction per bunch crossing, μ , is 1.5×10^{-2} . In this case, the probability a RHICf event occurs within $2 \mu\text{sec}$ after an event can be estimated as $1 - (1 - \mu\xi)^{(2\mu s/100 ns)} \sim 20\mu\xi = 1.8 \times 10^{-4}$. Here a bunch interval 100 ns is assumed. This means signal overlap in the slow shaping amplifier is negligibly small. It is worth repeating that such events can be removed at the analysis level.

The DAQ inefficiency is estimated as following. Because our DAQ speed is limited at 1kHz, successive event within 1 ms are not recorded and makes inefficiency in the data taking. The probability of any event occurring within 1 ms after an event can be estimated as $1 - (1 - \mu\xi)^{(1 ms/100 ns)} \sim 0.085$. This means the DAQ inefficiency due to the slow readout system is at a 10% level and does not make significant effect.

The update of Tab.5.1 taken new information above is given in Tab.A.1. For the 500 GeV p-p collisions, our ideal luminosity can be achieved with the conditions described in ‘RHIC Collider Projections’ and our first proposal. However the DAQ inefficiency amounts to 64%. The effect of non-negligible inefficiency is included in the time estimate in Tab.A.1.

Table A.1: Summary of assumption and requests for beam parameters

	Unit	p-p		p-N (p side)
		500 GeV	200 GeV	200 GeV
RHICf acceptance (ξ)		0.032	5.9×10^{-4}	4.5×10^{-4}
σ_{ine}	mb	50	40	330
emittance (ϵ)	mm mrad	20	<20	<20
β^*	m	10	>10	>10
luminosity (L)	$10^{30} \text{ cm}^{-2} \text{ s}^{-1}$	0.62	3.0	0.5
number of bunches (n_b)		6	100	100
N_{ine} per bunch crossing (μ)		6.5×10^{-2}	1.5×10^{-2}	2.1×10^{-2}
RHICf event rate ($\xi \sigma_{ine} L$)	Hz	10^3	71	74
RHICf event pileup ($\mu \xi$)		2.1×10^{-3}	8.9×10^{-6}	9.5×10^{-6}
RHICf event overlap ($20 \mu \xi$)		—	1.8×10^{-4}	1.9×10^{-4}
RHICf DAQ inefficiency (η_{ineff})		0.64	0.085	0.090
number of RHICf event (N_{RHICf})		10^6	10^6	10^6
number of collision (N_{ine})	10^8	0.31	17	22
integrated luminosity	nb^{-1}	0.63	42	6.7
total time ($N_{ine}/\sigma_{ine}/L/(1-\eta_{ineff})$)	hour	0.77	4.3	4.1